

# Investigation of Carrier Recombination Dynamics of InGaP/InGaAsP Multiple Quantum Wells for Solar Cells via Photoluminescence

K. -H. Lee, K. W. J. Barnham, John S. Roberts, D. Alonso-Álvarez, N. P. Hylton, M. Führer, N. J. Ekins-Daukes

**Abstract**—The carrier recombination dynamics of InGaP/InGaAsP quantum wells are reported for the first time. By studying the photoluminescence (PL) and time-resolved PL decay of InGaP/InGaAsP multiple-quantum-well(MQW) heterostructure samples, it is demonstrated that InGaP/InGaAsP MQWs have very low non-radiative recombination rate and high radiative efficiency compared to the control InGaP sample. Along with the analyses of PL emission spectrum and external quantum efficiencies, it suggests that this is due to small confinement potentials in the conduction band but high confinement potentials in the valence band. These results explain several features found in InGaP/InGaAsP MQW solar cells previously.

## I. INTRODUCTION

A novel InGaP/InGaAsP quantum well for tuning the absorption edge of the InGaP solar cell has been patented and implemented in commercial triple-junction solar cells[1][2]. The main advantage of InGaAsP as the well material for top cell is that one can change both the compositions of group III and V elements simultaneously to tune the band gap while maintaining a fixed lattice constant. JDSU has demonstrated that triple junction solar cells with dual-MQWs can achieve over 41% efficiency at 500 suns[2]. Studies of this MQW structure were also reported in several publications[3][4], mainly through external quantum efficiencies (EQE), I-V characteristics and detailed balance calculations. It was shown that this MQW has high external radiative efficiencies by measuring the photon coupling efficiency, however, the EQE of this MQW does not seem to be very efficient compared to GaAsP/InGaAs MQW solar cell.

In order to resolve these issues, we performed detailed temperature-dependent photoluminescence experiments to investigate the carrier dynamics of in the MQWs. We present a comparison between an InGaP/InGaAsP MQW and bulk InGaP control heterostructure sample. We further present the results from temperature dependent time-resolved PL decay and extract the effective recombination coefficients by fitting the experimental data with a rate model.

K. -H. Lee was with Department of Physics, Imperial College London, London, United Kingdom. He is currently with Toyota Technological Institute, Nagoya, Japan.

K. W. J. Barnham, D. Alonso- Álvarez, N. P. Hylton, M. Führer and N. J. Ekins-Daukes are with Department of Physics, Imperial College London, London, SW7 2AZ, United Kingdom.

John S. Roberts is with EPSRC National Centre for III-V Technologies, Sheffield, S3 7HQ, United Kingdom.

Table I  
LAYER STRUCTURES OF TS1111 AND TS1114. THE NOMINAL LAYER STRUCTURE OF THE QWS ARE 13.1-NM INGaP BARRIERS AND 4.4-NM  $\text{In}_{0.38}\text{Ga}_{0.62}\text{As}_{0.34}\text{P}_{0.66}$  WELLS.

layer name	TS1111	TS1114	thickness(nm)
cap	$\text{In}_{0.52}\text{Ga}_{0.48}\text{P}$	$\text{In}_{0.52}\text{Ga}_{0.48}\text{P}$	5.8
cladding	$\text{Al}_{0.59}\text{In}_{0.41}\text{P}$	$\text{Al}_{0.59}\text{In}_{0.41}\text{P}$	30
active layer	20xQWs	$\text{In}_{0.52}\text{Ga}_{0.48}\text{P}$	348
cladding	$\text{Al}_{0.59}\text{In}_{0.41}\text{P}$	$\text{Al}_{0.59}\text{In}_{0.41}\text{P}$	45
substrate	GaAs	GaAs	

## II. EXPERIMENT AND ANALYSIS

Two undoped heterostructure samples, TS1111 and TS1114 were fabricated to study the material properties of InGaP/InGaAsP quantum wells. The sample structures are listed in Table I. TS1111 has 20 repeats of InGaP/InGaAsP quantum wells as the active layer, which has 20 repeats of 4.4-nm InGaAsP wells separated by 13.1-nm InGaP barriers. The thicknesses and compositions of the MQWs are comparable to earlier devices reported in [2][5] and result in similar transition energies. The control sample, TS1114, is composed of bulk InGaP with the same active layer thickness as TS1111. Both samples were grown on GaAs substrates misorientated by 10 degrees towards the (001) plane to form disordered InGaP. The structures were grown using metalorganic chemical vapor deposition (MOCVD) and described in more detail in [1]. The compositions of InGaAsP and InGaP are designed to be lattice-matched to GaAs.

The samples were excited by a PicoQuant diode pulsed laser with emission wavelength at 485 nm with a repetition rate of 80 MHz, and a pulse duration of a few hundreds picoseconds. The average power of the laser beam was 4 mW, and the beam focused onto the test sample was close to a Gaussian profile with  $1/e^2$  radius of 49  $\mu\text{m}$ . This gives the injection density at the Gaussian peak of  $1.27 \times 10^{12} \text{ cm}^{-2}$ . The PL spectrum was dispersed using a Princeton Instrument SP2500 monochromator and detected using a silicon photodetector through a Stanford Research SR530 lock-in amplifier. The data was subsequently corrected to account for the spectral response of the detector and monochromator.

### A. Steady-state PL

The normalized PL spectra of TS1111 and TS1114 measured at temperatures between 30 K and 295 K are plotted in Figure 1(a) and (b). The peak PL photon energy of TS1111 is 1.69 eV at room temperature which is comparable to the

absorption edge reported in [5]. The peak PL photon energy of TS1114 is around 1.9 eV at room temperature, which is a characteristic of disordered InGaP. We note that ordered InGaP typically shows room temperature PL around 1.82 eV [6][7][8].

Figure 1(c) shows the spectrally integrated, normalized PL. The spectrally integrated PL of TS1111 saturates at temperatures below 200 K, suggesting that non-radiative recombination process do not play a dominant role in this temperature range. Also, a comparison of the absolute magnitude of the PL emission from the two samples shows that their integrated PL intensities are similar at 30 K. Thus we infer that the recombination in both samples is likely to be highly radiative at low temperatures. The radiative efficiency at room temperature, which is defined as the ratio between the radiative recombination and the overall recombination of electron-hole pairs, can be estimated as the ratio of the spectrally integrated PL at room temperature and low temperature. By this measure, the radiative efficiency of TS1111 at room temperature is found to be 84%, while the radiative efficiency of TS1114 is only 20%. The radiative efficiency of TS1111 is comparable to the values reported in [5], which was obtained from measurements of the photon coupling efficiencies of dual-MQW dual-junction devices. In [5], the highest measured photon coupling efficiency of the MQW InGaP cell is 52%, which results in a radiative efficiency of 68%. The temperature dependent PL was fitted using the rate model described in [9]. The fitted activation energy of TS1111 and TS1114 are 0.16 eV and 0.065 eV, respectively. The measured radiative efficiency of TS1111 is higher than the values measured in [5] because the instantaneous injection intensity is higher and there are no emitter or base layers which cause additional recombination losses, i.e. here we measure the internal quantum efficiency of the MQWs only, not a complete device. Figure 1(d) presents a plot of the PL full width at half maximum height, showing that the emission of TS1111 is very broad. This will be discussed further in the next section.

### B. TRPL decay

TRPL decay curves at the PL peak wavelengths were measured by time-correlated single photon counting to further study the recombination mechanisms of these samples. TRPL decay of TS1111 and TS1114 were illuminated at the same pulse power and beam size described in the previous section, but the repetition rate is reduced to a few MHz in order to measure longer decay times. The measured PL decays are plotted in Figure 2.

The PL decay is determined by the instantaneous excess carrier density, which can be described by the rate equation[10]:

$$\frac{\partial \sigma_n}{\partial t} = -A\sigma_n - \frac{B}{w}\sigma_n^2 - \frac{C}{w^2}\sigma_n^3 + D\nabla^2\sigma_n \quad (1)$$

The linear term coefficient  $A$  is the function of Shockley-Read-Hall recombination, surface recombination and monomolecular recombination,  $B$  is bimolecular radiative recombination coefficient,  $C$  is the coefficient that relates to Auger recombination and  $D$  is the diffusion coefficient of the carriers, and  $\sigma_n$  is the excess sheet carrier density.[11]

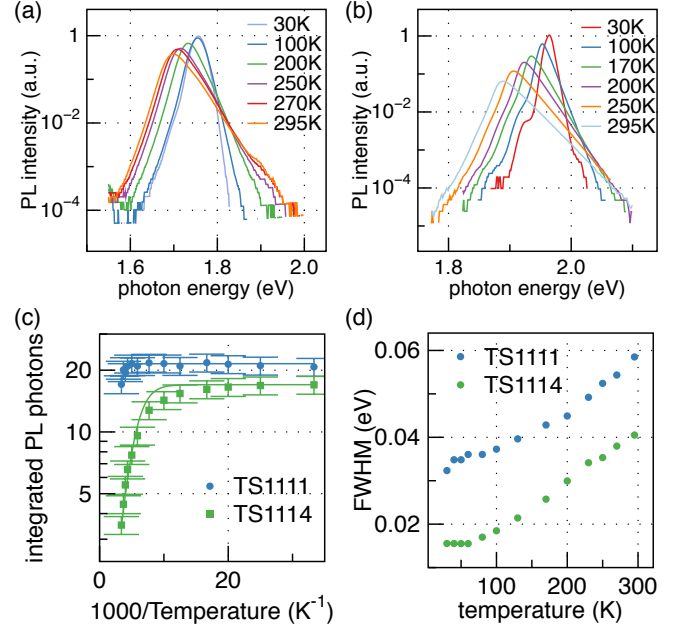


Figure 1. The PL spectrum of (a)TS1111 and (b)TS1114. The y-axes of both figures are normalized to the maximum intensities of each sample. (c) and (d) are spectrally integrated PL and the full-width half maximum of the PL, respectively. The solid lines in (c) are fittings using equation (2) in [9]. The fitted activation energies of TS1111 and TS1114 are 0.16 eV and 0.065 eV, respectively.

This assumes that the excited carriers are distributed uniformly within an effective layer of thickness  $w$ , and the recombination coefficients  $A$ ,  $B$  and  $C$  are constant throughout the PL decay. Although separating the contributions of the real recombination coefficients and photon re-absorption factors is difficult, it is the effective recombination rates,  $A$ ,  $B$  and  $C$ , that are of the most interest for devices since they are directly linked to the diffusion length of the carriers. Denoting  $B_s \equiv B/w$  and  $C_s \equiv C/w^2$ , the recombination coefficients  $A_s$ ,  $B_s$  and  $C_s$  can be retrieved by solving the rate equation to fit the TRPL decay data.

The diffusion coefficient of lowly-doped InGaAsP/InP QWs is reported to be of the order of few  $\text{cm}^2\text{sec}^{-1}$  at room temperatures[10][12]. The effect of diffusion at this level is found to be negligible in the decay time scale considered here. The difference of fitted  $A_s$  due to varying  $D$  from zero to  $10 \text{ cm}^2\text{sec}^{-1}$  is around  $10^5 \text{ sec}^{-1}$ , and the difference of fitted  $B_s$  caused by varying  $D$  in the same range is negligible.

In most cases, setting the coefficient of the third-order term  $C$  to be zero yields reasonable fit, suggesting that the Auger recombination is negligible.

The effective layer of thickness  $w$  of TS1111 and TS1114 need to be considered respectively due to different carrier redistribution mechanisms in bulk and MQWs. Since both InGaP and InGaAsP have the absorption coefficients around  $1.5 \times 10^5 \text{ cm}^{-1}$  at the laser wavelength[13][14], 64% ( $\sim 1 - 1/e$ ) of the carriers are absorbed in the first 75 nm of the active layer of both samples, so this value can be regarded as a lower limit of  $w$  for both samples. For TS1111, most of the carriers are captured and recombine in the quantum

well, showing that the carriers are transferred from one well to another by thermal escape or photon re-absorption. Therefore,  $w$  of TS1111 has a range from few wells to the total thickness of 20 wells depending on how uniform that the carriers are distributed. For TS1114, the excess carriers are redistributed by diffusion. The diffusion length of the carriers is  $\sim 700$  nm, based upon a diffusion coefficient of  $1 \text{ cm}^2\text{sec}^{-1}$  and the carrier lifetime is just 5 ns, so we can assume that the excess carriers in TS1114 are redistributed within the whole bulk InGaP layer. As a result,  $w$  of TS1114 can be estimated as the whole active layer thickness.

With the approximations and assumptions mentioned above, (1) can be solved using the laser profile as the initial condition of  $\sigma_n(r)$ . The total PL decay can then be calculated from the solution  $\sigma_n(r, t)$  using the relation[11]:

$$\phi \propto B_s \int_A \sigma_n(r) [(\sigma_n(r) + \sigma_D)] dA \quad (2)$$

where  $\sigma_D$  is the sheet background doping density of the samples. The background doping concentration  $N_D$  is of the order of  $\sim 10^{15} \text{ cm}^{-3}$ . The sheet background doping density can thus be written as  $\sigma_D = N_D w$ , which gives a sheet background doping density  $\sigma_D$  an upper bound  $\sim 10^9 \text{ cm}^{-2}$  by taking  $w$  as the thickness of the whole active layers. Since the excess density range covered by this TRPL decay measurement is from  $10^9$  to  $10^{12} \text{ cm}^{-2}$ , we have  $\sigma_n(r) \gg \sigma_D$ . (2) thus becomes

$$\phi \propto B_s \int_A \sigma_n^2(r) dA \quad (3)$$

The fitted TRPL decay and the fitted values are plotted in Figure 2 and Figure 3. This model fits the PL decay well at most timescales. However, the long lived tails of the experimental PL decay are not fitted very well, which may be due to the occupancies of long-lived trap states in the samples that slow the non-radiative recombination rates at late stage of the decay.

The fitted  $B_s$  of TS1111 is of the order of  $10^{-4} \text{ cm}^2/\text{sec}$ , thus the radiative recombination coefficient  $B$  is between  $10^{-11}$  to  $10^{-10} \text{ cm}^3/\text{s}$ , depending on the exact value of  $w$ . The range of  $B$  is comparable to the radiative recombination coefficients of InP/InGaAsP MQWs reported in [10], [15] and [16]. Also, the fitted  $B_s$  of both TS1111 and TS1114 drop as the temperature increases, because spontaneous radiative recombination rates becomes higher and  $w$  become lower as the temperature decreases.

The fitted  $A_s$  of TS1111 and TS1114 have different trends. Below 100 K, the fitted  $A_s$  of TS1114 increases with temperature, and then stays at the same level above 100 K. This result suggests that  $A_s$  of TS1114 is dominated by non-radiative recombination, which generally increases with temperature. However, the fitted  $A_s$  of TS1111 decreases with temperature, which suggests that radiative recombination is still dominant at high temperatures. This matches the qualitative behavior of the TRPL decays shown in Figure 2. When the carrier injection density  $n$  is low or the  $A$  coefficient is high ( $A \gg Bn$ ), the PL decay is dominated by the term  $An$  and therefore is a straight line in the logarithmic plot. In contrast, if the

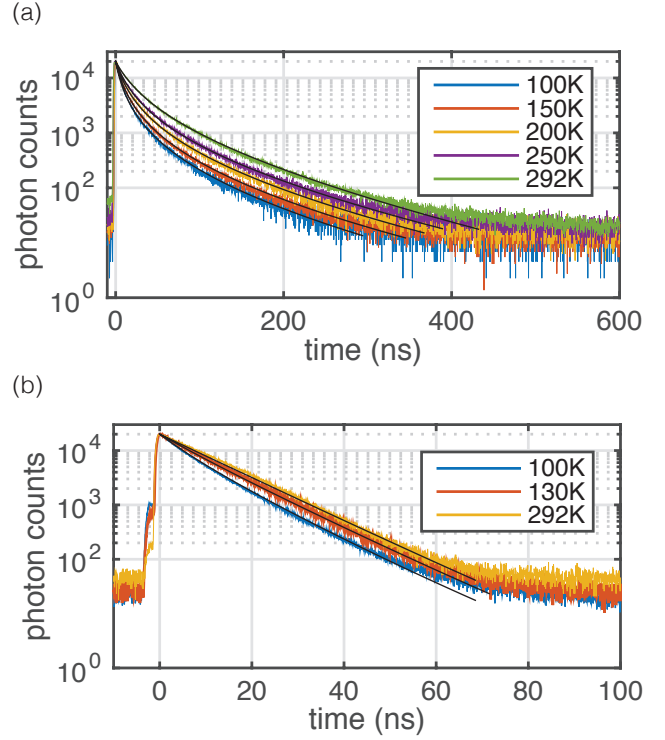


Figure 2. Measured and fitted TRPL decays of (a)TS1111 and (b)TS1114 at various temperatures.

carrier density  $n$  is high or  $A$  is low ( $A \ll Bn$ ), the decay will not be single-exponential and the instantaneous decay rate will change with the remaining excess carrier densities. Therefore, at high carrier density, the initial decay of the TRPL is dominated by radiative recombination and dependent on  $B$  and  $n$ , and the decay rate in the late stage is determined by  $A$ . At low temperature, both TS1111 and TS1114 has non-single-exponential PL decay. However, at high temperatures, TS1114 is dominated by single-exponential decay but TS1111 is still non-single-exponential, suggesting that TS1111 has a much lower  $A$  coefficient.

The  $A_s$  coefficient of TS1111 is around  $10^6 \text{ sec}^{-1}$ , which is one order of magnitude lower than TS1114 at all temperatures. Since  $A_s$  is the upper limit of the non-radiative recombination rates, this supports the observation of the steady-state PL that the quantum well sample has much higher radiative efficiency than the bulk sample.

In [10], the  $A_s$  of undoped InP/InGaAsP MQWs at room temperature is reported to be  $2 \times 10^5 \text{ sec}^{-1}$ , which is one order of magnitude lower than the fitted  $A_s$  of TS1111. This suggests that the quality of InGaP/InGaAsP MQWs is not as high as InP/InGaAsP MQWs.

### III. DISCUSSION

In summary, the radiative efficiency of the InGaP/InGaAsP MQWs obtained from PL measurement is high, and this is consistent with the observed trend of  $A_s$  against temperature. In addition, the fitted recombination rate  $B_s$  of the MQW sample is much lower than the control sample. Also, the

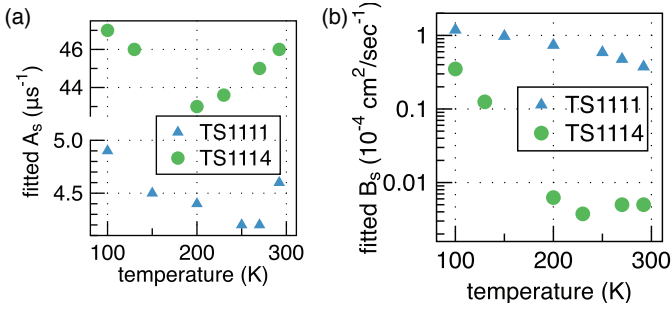


Figure 3. The fitted values of  $A_s$  and  $B_s$  of TS1111 and TS1114 in (1).

FWHM of this MQW sample's PL emission is broader than the PL emission of the control sample.

The broad PL emission of MQW sample is consistent with the modest onset of the absorption near the band-edge evident from the external EQE of this MQW InGaP cell. Figure 4 shows the EQE and absorption coefficients of a dual-MQW dual-junction solar cell reported in [17]. This cell has a top cell that has MQWs with same design as TS1111 and a GaAs bottom cell with GaAsP/InGaAs MQWs. The absorption coefficients are calculated from EQEs by assuming a infinite diffusion length, i.e.,

$$\alpha(E) = -\log(1 - \text{EQE}(E))/L \quad (4)$$

where  $\alpha(E)$  is the absorption coefficient,  $E$  is the photon energy, and  $L$  is the thicknesses of the total MQWs layer. We can observe that the absorption edge of the bottom cell's MQW is much sharper than the top cell's MQW. This suggests a tail of states in the QW or type II transitions[18]. It is worth noted that this characteristic of EQE can also be found in this type of MQW cell fabricated by other facilities, such as the ones reported in [2].

This feature can be explained by an approximation of band alignment using electron affinities. The electron affinity of InGaAsP can be approximated by interpolation [19]:

$$Q(x, y) = (1 - x)yB_{\text{InAs}} + xyB_{\text{GaAs}} + (1 - x)(1 - y)B_{\text{InP}} + x(1 - y)B_{\text{GaP}} \quad (5)$$

where  $B_{\text{InAs}}$ ,  $B_{\text{GaAs}}$ ,  $B_{\text{InP}}$  and  $B_{\text{GaP}}$  are the parameters of InAs, GaAs, InP, and GaP listed in Table II.

Figure (5) shows the band gaps and lattice constants of  $\text{In}_{1-x}\text{Ga}_x\text{As}_y\text{P}_{1-y}$  as the function of Ga and As compositions respectively. The dashed line in Figure (5)(b) represent the combination of  $x$  and  $y$  that keeps its lattice constant equal to GaAs (5.64 Å). As shown in the figure, this line almost overlaps with the contour of 4.1 eV, which is very close to the electron affinity of GaAs and InGaP. This suggests that the confinement potential of electrons in the quantum well is small, which causes the slow onset of absorption as shown in Figure 4.

This argument can also explain the fitted activation energy of TS1111 (0.16 eV). This value is close to the difference between the peak PL wavelengths of TS1111 and TS1114. Since the result of TRPL shows that the MQW is very radiative, the fitted activation energy should correspond to the energy barrier for carrier escape from the well to the

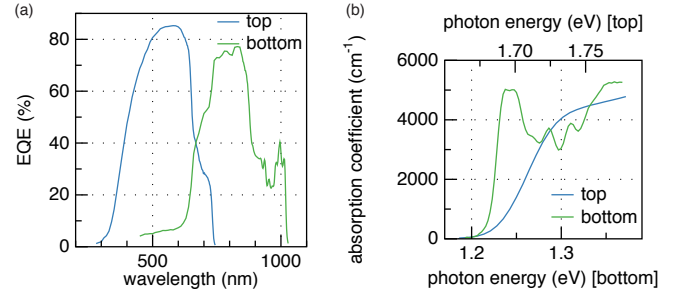


Figure 4. The (a) measured EQE and (b) extracted absorption coefficients of the subcells in the dual-MQW dual-junction device described in [17].

Table II  
THE MATERIAL PARAMETERS OF THE BINARY MATERIALS FOR ESTIMATING THE BAND GAPS, ELECTRON AFFINITIES AND LATTICE CONSTANTS OF INGAASP[19].

	band gap (eV)	lattice constants (Å°)	electron affinity (eV)
GaP	2.776	5.4512	3.8
GaAs	1.415	5.6533	4.07
InP	1.35	5.8688	4.38
InAs	0.36	6.0584	4.9

barrier. As a result, either the confinement potential in the conduction band or valence band is large whereas the other one is small. The estimation of electron affinities suggest that it is the confinement potentials in the valence band that accounts for this activation energy.

#### IV. CONCLUSIONS

The carrier recombination dynamics of InGaP/InGaAsP multiple quantum wells is presented for the first time. The spectrally integrated PL shows that InGaP/InGaAsP MQWs can achieve 84% radiative efficiency at high excitation, which is comparable to the estimations obtained from fitting the dark currents and direct measurement of the radiative coupling in [3] and [5] respectively. In addition, the temperature dependent recombination coefficients show that the MQWs at same excitation levels as PL experiment is radiative dominant across the whole temperature range, while the bulk InGaP sample is dominated by non-radiative recombination. Along with the observations of PL spectrum and spectrally integrated PL,

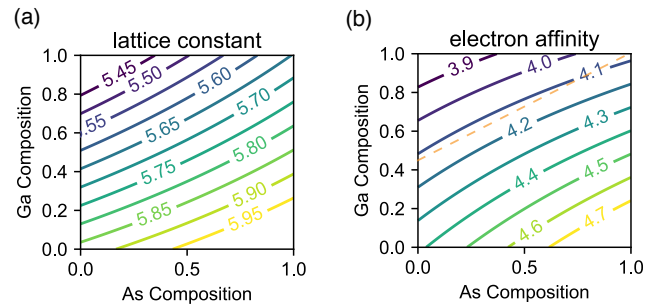


Figure 5. The calculated (a) lattice constant(Å°) and (b) electron affinity (eV) contours of  $\text{In}_{1-x}\text{Ga}_x\text{As}_y\text{P}_{1-y}$  as a function of  $x$  and  $y$  using Eq. (5) and the parameters in Table II. The orange dashed line in (b) represent the  $\text{In}_{1-x}\text{Ga}_x\text{As}_y\text{P}_{1-y}$  lattice-matched to GaAs.

this result indicates that non-radiative recombination in the MQWs is suppressed by the quantum confinement potentials in the wells. The estimated electron affinity suggests that strong quantum confinement potentials mainly come from the valence band, which is consistent to the activation energy of non-radiative recombination obtained by temperature-dependent PL.

#### ACKNOWLEDGMENTS

This work is partly supported by QuantaSol Ltd. and the European Commission within the FP7 Research Framework Program NGCPV.

#### REFERENCES

- [1] J. Roberts, "PHOTOVOLTAIC CELL," Patent 13/121,364, Mar., 2011.
- [2] B. Browne, J. Lacey, T. Tibbits, G. Bacchin, T.-C. Wu, J. Q. Liu, X. Chen, V. Rees, J. Tsai, and J.-G. Werthen, "Triple-junction quantum-well solar cells in commercial production," *AIP Conference Proceedings*, vol. 1556, pp. 3–5, Dec. 2013.
- [3] K. W. J. Barnham, B. C. Browne, J. P. Connolly, J. Adams, R. J. Airey, N. J. Ekins-Daukes, M. Führer, V. Grant, K.-H. Lee, M. Lumb, M. Mazzer, J. S. Roberts, and T. N. D. Tibbits, "Photonic Coupling in Multi-Junction Quantum Well Concentrator Cells," in *The 25th European Photovoltaic Solar Energy Conference and Exhibition Proceedings*, Sep. 2010, pp. 234–240.
- [4] J. G. J. Adams, B. C. Browne, I. M. Ballard, J. P. Connolly, N. L. A. Chan, A. Ioannides, W. Elder, P. N. Stavrinou, K. W. J. Barnham, and N. J. Ekins-Daukes, "Recent results for single-junction and tandem quantum well solar cells," *Progress in Photovoltaics: research and applications*, vol. 19, no. 7, pp. 865–877, Jan. 2011.
- [5] K.-H. Lee, K. W. J. Barnham, J. P. Connolly, B. C. Browne, R. J. Airey, J. S. Roberts, M. Führer, T. N. D. Tibbits, and N. J. Ekins-Daukes, "Demonstration of Photon Coupling in Dual Multiple-Quantum-Well Solar Cells," *Photovoltaics, IEEE Journal of*, vol. 2, no. 1, pp. 68–74, Jan. 2012.
- [6] Y. C. Yeo, M. F. Li, T. C. Chong, and P. Y. Yu, "Theoretical study of the energy-band structure of partially CuPt-ordered  $\text{Ga}_{0.5}\text{In}_{0.5}\text{P}$ ," *Physical Review B*, vol. 55, no. 24, pp. 16 414–16 419, Jun. 1997.
- [7] F. P. Dabkowski, P. Gavrilovic, K. Meehan, W. Stutius, J. E. Williams, M. A. Shahid, and S. Mahajan, "Disordering of the ordered structure in metalorganic chemical vapor deposition grown  $\text{Ga}_{0.5}\text{In}_{0.5}\text{P}$  on (001)GaAs substrates by zinc diffusion," *Applied Physics Letters*, vol. 52, no. 25, pp. 2142–2144, 1988.
- [8] R. B. Capaz and B. Koiller, "Partial-ordering effects in  $\text{In}_x\text{Ga}_{1-x}\text{P}$ ," *Physical Review B*, vol. 47, no. 7, pp. 4044–4047, Feb. 1993.
- [9] J. D. Lambkin, D. J. Dunstan, K. P. Homewood, L. K. Howard, and M. T. Emeny, "Thermal quenching of the photoluminescence of InGaAs/GaAs and InGaAs/AlGaAs strained-layer quantum wells," *Applied Physics Letters*, vol. 57, no. 19, pp. 1986–1988, Nov. 1990.
- [10] J. M. Smith, G. S. Buller, D. Marshall, A. Miller, and C. C. Button, "Microsecond carrier lifetimes in InGaAsP quantum wells emitting at  $\lambda=1.5\text{ }\mu\text{m}$ ," *Applied Physics Letters*, vol. 80, no. 11, pp. 1870–1872, Mar. 2002.
- [11] R. K. Ahrenkiel, "Minority-Carrier Lifetime in III–V Semiconductors," in *Semiconductor and Semimetals*. Elsevier, 1993, pp. 39–150.
- [12] D. Marshall, A. Miller, and C. C. Button, "In-well ambipolar diffusion in room-temperature InGaAsP multiple quantum wells," *Quantum Electronics, IEEE Journal of*, vol. 36, no. 9, pp. 1013–1015, 2000.
- [13] Y. A. Goldberg, "Gallium Indium Arsenide Phosphide," in *Handbook Series on Semiconductor Parameters*, 1996, pp. 153–179.
- [14] —, "Gallium Indium Phosphide," in *Handbook Series on Semiconductor Parameters*, 1996, pp. 37–61.
- [15] A. M. Fox, R. J. Manning, and A. Miller, "Picosecond relaxation mechanisms in highly excited GaInAsP," *Journal of Applied Physics*, vol. 65, no. 11, pp. 4287–4298, Jun. 1989.
- [16] E. Wintner and E. P. Ippen, "Nonlinear carrier dynamics in  $\text{Ga}_x\text{In}_{1-x}\text{As}_y\text{P}_{1-y}$  compounds," *Applied Physics Letters*, vol. 44, no. 10, pp. 999–1001, 1984.
- [17] K.-H. Lee, K. W. J. Barnham, J. S. Roberts, M. Führer, D. Alonso-Alvarez, and N. J. Ekins-Daukes, "Dual-junction solar cells with multiple-quantum-well top cells," *AIP Conference Proceedings*, vol. 1556, pp. 45–47, Dec. 2013.
- [18] G. Bastard, "Optical properties of quasi-bimimensional systems," in *Wave mechanics applied to semiconductor heterostructures*. Wiley-Interscience, 1988, p. 237.
- [19] S. Adachi, "Material parameters of  $\text{In}_{1-x}\text{Ga}_x\text{As}_y\text{P}_{1-y}$  and related binaries," *Journal of Applied Physics*, vol. 53, no. 12, pp. 8775–8792, Dec. 1982.